BIOCHEMISTRY
including biophysical chemistry & molecular biology
Article

Biochemistry **2009,** *48,* 9903–9911 9903
DOI: 10.1021/bi901352m

Real Time Monitoring of Sickle Cell Hemoglobin Fiber Formation by UV Resonance Raman Spectroscopy[†]

Kelly M. Knee[‡] and Ishita Mukerji*

Molecular Biology and Biochemistry Department, Molecular Biophysics Program, Wesleyan University, Middletown, Connecticut 06459. [‡]Present address: Department of Biology, Massachusetts Institute of Technology, Cambridge, MA 02139

Received August 4, 2009; Revised Manuscript Received September 10, 2009

ABSTRACT: In sickle cell hemoglobin, individual tetramers associate into long fibers as a consequence of the mutation at the β6 position. In this study UV resonance Raman spectroscopy is used to monitor the formation of Hb S fibers in real time through aromatic amino acid vibrational modes. The intermolecular contact formed by the mutation site ($^1\beta_1$6 Glu→Val) of one tetramer and the $^2\beta_2$85 Phe−$^2\beta_2$88 Leu hydrophobic pocket on a different tetramer is observed by monitoring the increase in signal intensity of Phe vibrational modes as a function of time, yielding kinetic progress curves similar to those obtained by turbidity measurements. Comparison of individual spectra collected at early time points (< 1000 s) show small Phe intensity changes, which are attributed to weak transient associations of Hb S tetramers during the initial stages of the polymerization process. At later times (1000−2000 s) Phe signal intensity steadily increases because of increasing hydrophobicity of local Phe environment, a consequence of forming more stable $^1\beta_1-^2\beta_2$ contacts. Tyr and Trp vibrational modes monitor H-bond strength between critical residues at the $\alpha_1\beta_2$ interface of individual tetramers. Kinetic progress curves generated from these signals exhibit two distinct transitions at 2040 and 7340 s. These transitions, which occur later in time than those detected either by turbidity (1560 s) or by Phe signal intensity (1680 s), are attributed to initial fiber formation and subsequent formation of larger assemblies, such as macrofibers or gels. These results provide molecular insight into the interactions governing Hb S fiber formation.

Sickle cell disease is a genetic disorder caused by a single point mutation (β6 Glu→Val) in hemoglobin and is characterized by the association of deoxygenated sickle cell hemoglobin (Hb S)[1] tetramers into long polymers. The site of the mutation creates a hydrophobic patch on the protein surface, which can then interact with a different Hb S tetramer. This interaction between the $^2\beta_2$6 Val of one tetramer and the $^1\beta_1$85 Phe and $^1\beta_1$88 Leu residues of a different tetramer[2] is critical for fiber formation and is referred to as a donor−acceptor interaction (*1*−*3*). Accumulation of the sickle cell polymers deforms red blood cells into a sickled shape, leading to vaso-occlusion and other pathologies. Since sickle cell Hb only polymerizes in the deoxygenated state, therapies that inhibit polymerization must be able to act within the time scale of circulation, before reoxygenation (*4*). Thus, many effective treatment strategies have focused on delaying the initial steps of the polymerization process.

Hb S polymer formation has been successfully described by a double nucleation mechanism in which fiber formation occurs in two steps (*5*−*8*). Briefly, the overall process can be described in two main stages: The first stage is homogeneous nucleation where individual tetramers reversibly associate until a critical nucleus is achieved that is energetically stable. The second stage, heterogeneous nucleation, is a rapid, energetically favorable step when individual monomers are added to preexisting nuclei and fibers (*5*, *7*, *8*)

Recent lines of investigation have suggested that nucleation is preceded by the formation of metastable clusters in concentrated Hb S solutions. These metastable clusters, identified by differential interference contrast microscopy and dynamic light scattering, appear to be precursors to the formation of ordered nuclei and polymers (*9*−*14*). Hb S polymers have been shown to nucleate in these metastable clusters, and the rate of formation of the clusters limits the rate of nucleation (*13*). These observations suggest that the homogeneous nucleation step in the double nucleation mechanism potentially consists of the formation of mesoscopic metastable dense liquid clusters followed by ordered nucleation. Yet to be determined is the point at which molecular order is established within these clusters.

The structure and organization of hemoglobin fibers have been modeled using electron microscopy and X-ray crystallography, in which the overall dimensions are established by electron microscopy and the molecular interactions are inferred from the double strands observed in crystallographic data. In the X-ray crystal structure the overall quaternary structure of the Hb S tetramer is very similar to that of Hb A. A tertiary structural difference was observed in the tetramers, in which the A-helix containing the mutation is displaced toward the interior of the protein (*2*), which was later confirmed in solution by UV resonance Raman spectroscopy (*15*). The fibers are composed of seven

[†]This work was supported by grants from the Patrick and Catherine Weldon Donaghue Medical Research Foundation and the National Science Foundation (MCB-031665) (awarded to I.M.). An NIH Molecular Biophysics training grant, GM 008272, supported K.M.K.

*To whom correspondence should be addressed. Phone: 860-685-2422. Fax: 860-685-2141. E-mail: imukerji@wesleyan.edu.

[1]Abbreviations: DIC, differential interference contrast; ds, double strands; Hb, hemoglobin; Hb S, sickle cell hemoglobin; KP, potassium phosphate; UVRR, UV resonance Raman.

[2]In this format $^2\beta_2$ refers to subunit β_2 in tetramer 2 and $^1\beta_1$ refers to subunit β_1 in tetramer 1.

Published on Web 09/10/2009

half-staggered double strands, which are wound together in a ropelike fashion with a helical twist of approximately 7−9° (*16*, *17*). Analysis of diffraction patterns suggests that the double strands observed in the fibers and the crystals are similar, although the double strands in the crystal are linear and not twisted (*1*, *2*). In a comparison of the double strands from crystals and fibers, the β6 lateral contacts remain relatively intact in both structures, while the axial interactions are reduced because of the helical twist and the length of the strands (*18*). Over time, the fibers evolve to form higher order polymer structures, such as macrofibers at low pH (*19*, *20*), and bunched and branched fibers at higher pH (*20*−*22*). At physiological pH over time the fibers will spontaneously convert to the crystal.

Recently, the spectroscopic technique of UV resonance Raman spectroscopy (UVRR) is emerging as a powerful method for studying protein structure and dynamics under different conditions (*23*−*30*). In the case of Hb, for example, spectroscopic signals diagnostic of quaternary states have been identified, and the evolution of these signals as a function of time has led to a mechanistic understanding of the T to R transition (*25*, *31*−*36*). Since the technique does not rely on the solution state and is not size limited, it has been successfully applied to the study of fiber formation. Specifically, UVRR spectra of Hb S fibers under equilibrium conditions have revealed new insight into the structural features of the fiber state (*37*, *38*). The different fibrillar states of lysozome have also been studied effectively using this technique, and these studies have elucidated sequential events of protein conformational changes leading to formation of the critical nucleus (*39*, *40*).

In this work nucleation and fiber formation in Hb S are monitored using UVRR spectroscopy in real time. The intermolecular $^1\beta_1-^2\beta_2$ interactions are detected using the Phe vibrational signal, which has been shown to increase in intensity with the formation of fibers (*37*, *38*). Spectroscopic signals corresponding to the β37 Trp and α42 Tyr residues are used to monitor H-bond interactions that stabilize the intersubunit interface of individual tetramers (*25*, *33*, *41*). These spectroscopic signals, monitored as a function of time, yield kinetic progress curves similar to those obtained by turbidity. The curves, as obtained from the Raman data, yield distinct time constants for intermolecular and intramolecular interactions. Overall, these findings reveal new molecular insights into the association of double strands and mechanism of Hb S fiber formation.

MATERIALS AND METHODS

Hemolyzate Isolation. Sickle cell Hb was isolated from the blood of SS and SC patients. Hemolyzate extraction was performed using the method described by Antonini and Brunori (*42*).

Deoxy Hb S Formation. Approximately 500−1000 μL of 0.25 mM CO Hb S (1.0 mM heme) in 1.25 M potassium phosphate buffer, pH 7.1, and 10 mM sodium dithionite was kept in a rotating 100 mL round-bottom flask and photolyzed with a 500 W halogen lamp under N_2 at 4 °C for 1.5 h to prepare deoxy Hb S samples. Following photolysis, the samples were transferred to either 1 mm path length glass cuvettes or 1.5 mL glass vials, which had been N_2 purged for at least 30 min. The samples were maintained in the deoxygenated state, and the concentration of the samples was determined by visible absorbance; samples containing greater than 5% methemoglobin were discarded.

Kinetics of Hb S Fiber Formation. The rate of Hb S fiber formation was determined by turbidity measurements. Fiber formation was initiated by temperature jump from 10 to 25 °C. The change in absorbance at 700 nm was monitored at 32 s intervals for 6000−10000 s using a Beckman DU 650 spectrophotometer. Absorbance curves were fit using the equation:

$$y = \frac{A_1 - A_2}{1 + e^{(x - x_0)/dx}} + A_2$$

where A_1 and A_2 are the initial and final absorbance, x is time, and x_0 is the time point at which 50% of the total absorbance change has occurred. The initial 15% of the polymerization curves were also fit to the equation:

$$y = A_0 + (A_f(A_{max} - A_0))(\cosh(Bt) - 1)$$

which is the result from the integration of the linearized rate equations of the double nucleation mechanism (*5*, *43*), where A_0 and A_{max} are the initial and final absorbances, A_f and B are the shape and rate parameters used to define the initial portion of the polymerization curve and t is time. Reported values result from an average of at least three independent experiments.

Steady-State UV Resonance Raman Spectroscopy. A Q-switched, Nd:YLF pumped Ti:sapphire laser system (Quantronix, New York) was used to generate the excitation wavelengths by frequency quadrupling the IR output of the Ti:sapphire laser using two BBO crystals, as previously described (*15*). Data acquisition and analysis were done as described (*37*, *38*). For aggregation and melting experiments, deoxy samples were prepared, and steady-state spectra were collected with an acquisition time of 15 min, and the spectra shown represent at least 3 h of averaged data for steady-state measurements. Following polymerization, samples were allowed to cool to 4 °C, and a second set of steady-state data were collected.

Time-resolved UV resonance Raman experiments were performed by allowing deoxy Hb S samples at 4 °C to warm to room temperature in the Raman sample holder. The temperature of the sample was monitored during the warming process, and the sample reached room temperature in 4 min. Data were collected for 6000−10000 s with a 60 s integration time and 180 s between each acquisition. Data collected at the same time points from at least three independent experiments were averaged and used to generate error bars.

Data manipulation and analysis were performed using Grams AI spectral analysis software (ThermoGalactic, Salem, NH). Kinetic traces were generated by monitoring changes in frequency and intensity of specific vibrational modes as a function of time. Polymerization curves were analyzed as described for the kinetics of Hb S fiber formation.

RESULTS

The Hb S fiber formation process is strongly dependent on temperature, protein concentration, and phosphate concentration. In our study polymerization was initiated by a temperature jump from 5 to 25 °C. To establish the timing of the polymerization process under our spectroscopic conditions, we examined the fiber formation process under a number of different solution conditions by the increase in sample turbidity at 700 nm (Figure 1). At this wavelength there is little to no interference from either heme or protein absorption, and the absorbance increase arises from greater sample turbidity resulting from fiber formation. Measurements performed over the phosphate concentration range from 0.75 to 1.8 M yielded delay times in the 1900−1200 s range. As expected,

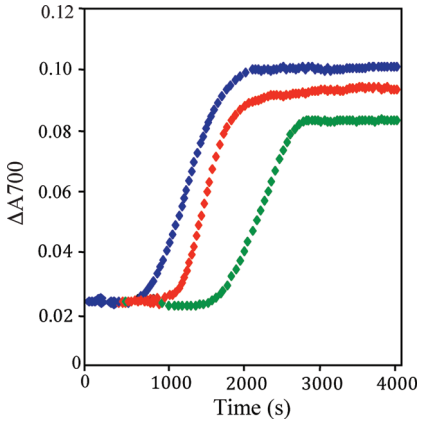

FIGURE 1: Kinetic progress curves for 0.25 mM (hemoglobin) Hb S at a range of KP concentrations from 1.8 M (blue) to 0.75 M (green). A concentration of 1.25 M KP (red) yielded the most consistent delay times and was therefore used in all the time-resolved UVRR experiments.

Table 1: Delay Times As Measured by Turbidity and UVRR Spectroscopy[a]

Turbidity Measurements at 700 nm		
	τ_d, 15%	τ_d, 50%
deoxy Hb S	1240 ± 80	1560 ± 100
seed nuclei or aggregates		
before cooling	1190 ± 60	1590 ± 80
after cooling	890 ± 70	1290 ± 90
UVRR Measurements		
Phe modes (cm^{-1})		τ_d
1604 (F8a)		1700 ± 80
1583 (F8b)		1740 ± 90
1180 (F9a)		1630 ± 70
1005 (F12)		1660 ± 110
Phe mode average		1680 ± 90
UVRR Measurements		
Tyr, Trp modes (cm^{-1})	τ_{d1}[b]	τ_{d2}[b]
1615 (Y8a)	2110 ± 140	7350 ± 180
1209 (Y7a)	1960 ± 180	7160 ± 170
1548 (W3)	2050 ± 150	7520 ± 180
Tyr, Trp mode average	2040 ± 160	7340 ± 180

[a]Delay times are reported for measurements performed at a Hb S concentration of 0.25 mM in a 1.25 M potassium phosphate buffer. Unless noted, delay times refer to the time point at which the signal has changed by 50%. [b]In the case of the Tyr and Trp modes, two delay times are reported because two transitions are observed. To obtain the delay times, the transitions are treated independently as described in the text.

longer delay times were observed at lower phosphate concentrations. The delay times observed as a function of phosphate concentration were consistent with previously reported values obtained at similar phosphate concentrations (*6*, *44*, *45*). To optimize the UVRR signal obtained and minimize absorption of the scattered light by the sample itself, the Hb S concentration was held constant at 0.25 mM Hb S. These conditions for UVRR experiments, 1.25 M phosphate and 0.25 mM Hb S, yielded a consistent delay time of 1560 ± 100 s (Table 1).

Direct Observation of the $^1\beta_1$–$^2\beta_2$ Interaction: Phe Residues. Excitation into the electronic excitation bands of

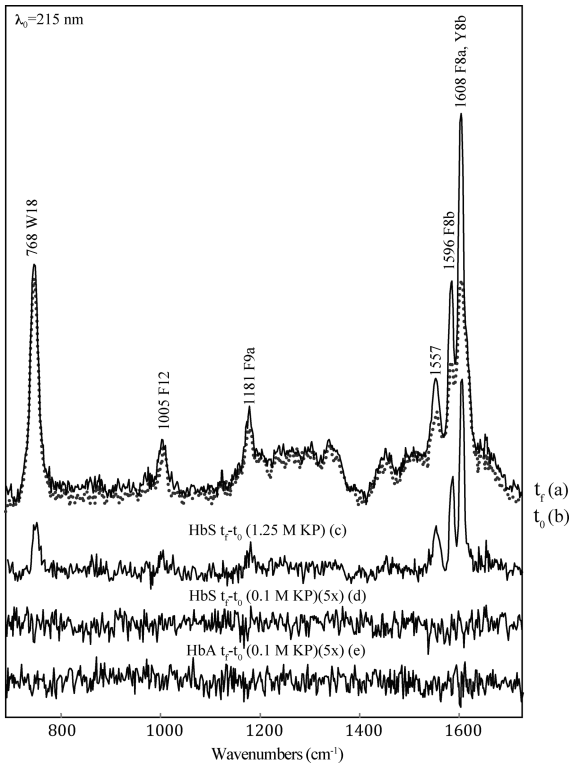

FIGURE 2: Time-resolved UVRR spectra of Hb S before initiation of polymerization (dashed line) and after polymerization (solid line), excited at 215 nm. Final minus initial difference spectra are also shown for Hb S under favorable polymerization conditions (0.25 mM Hb, 1.25 M KP), unfavorable polymerization conditions (0.25 mM Hb, 0.1 M KP), and for Hb A (0.25 mM Hb, 1.25 M KP). Intensity increases of the Phe modes are only observed for the Hb S sample under favorable polymerization conditions, suggesting that the increases result from fiber formation and not nonspecific protein aggregation.

different amino acid residues significantly enhances their vibrational signals. With an excitation wavelength of 215 nm, Phe residues are resonantly enhanced, making it possible to monitor the intermolecular $^1\beta_1$–$^2\beta_2$ interaction formed between the $^1\beta_1$ residues, 85 Phe and 88 Leu, and the mutant $^2\beta_2$6 Val residue. At the 215 nm excitation wavelength, the spectrum is dominated by Phe modes with some contributions from Tyr and amide vibrational modes associated with the peptide bond (*15*, *38*). Figure 2 shows the UVRR spectra of Hb S obtained at the initial time point (t_0) (0 s) and final time point (t_f) (5000 s). With fiber formation, the F8a and F8b vibrational modes, occurring at 1606 and 1585 cm^{-1}, show the greatest increase in intensity, and additional small intensity increases are observed for the F9a and F12 vibrational modes. The strong Trp vibrational mode, W18 at 768 cm^{-1}, also exhibits an increase in intensity with fiber formation (*vide infra*). The overall magnitude of the intensity increase is consistent with previously observed changes in Phe intensity associated with fiber formation, where the F8a and F8b modes experience the largest intensity increases as a function of increasing hydrophobicity (*37*, *38*). This increase in hydrophobicity is attributed to the formation of the $^1\beta_1$–$^2\beta_2$ contacts, which significantly reduces the solvent exposure of the β85 Phe residue, relative to that observed in the T-state (*1*, *2*, *46*). Thus, upon fiber formation the observed Phe signal is primarily attributed to the β85 Phe residue which experiences the greatest change in local environment.

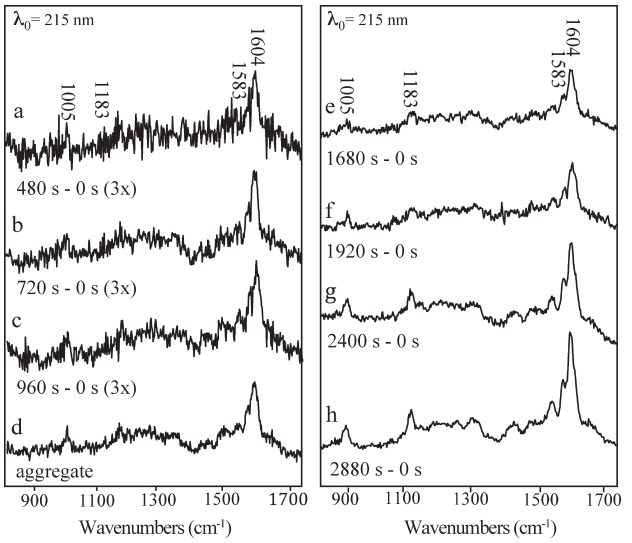

FIGURE 3: UVRR difference spectra generated between the initial time point spectra, t_0, and later time point spectra as indicated. Difference spectra generated between t_0 and early times (<1000) (panel a) show a small increase in Phe signal intensity, with a similar magnitude of intensity increase at all times. Difference spectra generated between t_0 and later times (>1000) (panel b) show a continuous increase in Phe signal intensity, suggesting an increase in the strength and number of intermolecular contacts as a function of time. The difference spectrum obtained with aggregates generated after one cycle of heating and cooling is shown at the bottom of panel a.

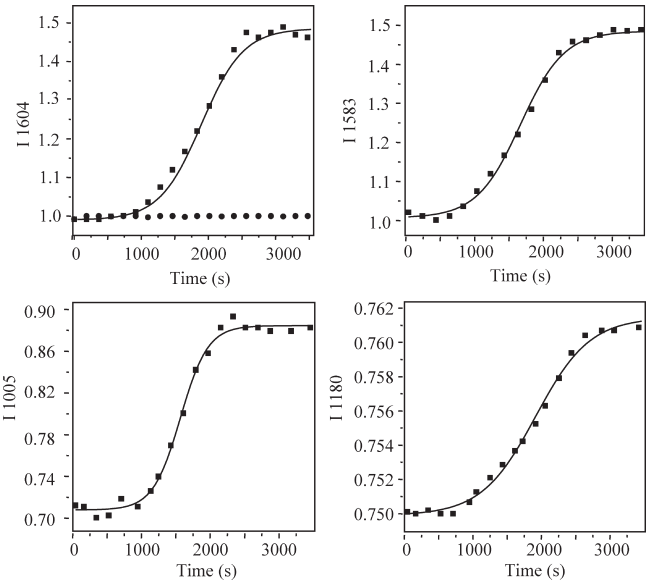

FIGURE 4: UVRR kinetic progress curves generated by monitoring the change in intensity of indicated Phe modes as a function of time using an excitation wavelength of 215 nm. Phe intensities at 1604, 1583, 1005, and 1180 cm^{-1} are shown in panels a, b, c, and d, respectively. Black circles in panel a show the intensity of the 1604 cm^{-1} mode as a function of time for 0.25 mM Hb A in the same solution conditions used for Hb S fiber formation. Solid black lines represent the associated Boltzmann fits.

Difference spectroscopy is used to identify only those features associated with fiber formation. The large increase in Phe signal intensity upon completion of polymerization can be seen in the $t_f - t_0$ difference spectrum (Figure 2c). This difference spectrum is comparable to steady-state fiber minus deoxy tetramer (F − T) difference spectra and confirms the presence of Hb S fibers (*37*, *38*). The UVRR difference spectrum of Hb A obtained under the same conditions (Figure 2e) is relatively featureless, demonstrating that the signal obtained is intrinsic to Hb S. Data are also shown for low phosphate conditions (0.1 M KP), where polymerization is not expected and the absence of polymerization is confirmed by the observance of a featureless difference spectrum (Figure 2d). At the concentrations of hemoglobin used, a relatively high concentration of phosphate buffer (0.75−1.25 M) is needed to induce Hb S polymerization (*47*−*49*). We have previously shown that UVRR signals of Hb S fibers obtained at low and high phosphate concentrations are indistinguishable (*37*), in good agreement with electron microscopy studies demonstrating fibers formed at low and high phosphate concentrations have the same structure (*20*).

Difference spectra generated as a function of time are shown in Figure 3. The t_0 spectrum is subtracted from the spectra obtained at specific times to reveal only those changes that occur as a function of time and are distinct from the initial state. These spectra demonstrate that after 1000 s Phe mode intensity increases with time, in good agreement with the increase in intensity observed in the steady-state F − T spectra (*37*, *38*). The magnitude of the intensity increase observed from 0 to 480, 720, or 960 s remains relatively constant (Figure 3), suggesting that in the initial stages of polymerization the aggregates are held together by weak, transient interactions. At later times it can be observed that the Phe intensity continually increases. This intensity increase at longer times (>1000 s) can be attributed to either an increase in the local hydrophobicity of the β85 Phe or an increase in the number of interactions. From comparison with turbidity data (Figure 1) the increase in intensity is attributed to an increase in the number of interactions and the association of tetramers into Hb S fibers. At the longest times (>2400 s), the magnitude of the intensity change is consistent with steady-state measurements.

Monitoring the change in signal intensity of the Phe modes as a function of time yields kinetic progress curves (Figure 4), similar to those obtained from turbidity measurements (Figure 1). From these curves, the time at which 50% (t_{50}) of the process has occurred can be obtained. The 50% times, which represent both homogeneous nucleation and rapid polymerization, were used for comparison, as there were insufficient points in the UVRR data to accurately determine the time at which 15% of the change had occurred as commonly used by others to characterize the delay time (*5*, *6*). The transition midpoints for the Phe modes are within error of each other and yield an average value of 1680 ± 90 s (Table 1). This value is in good agreement with the t_{50} of 1560 ± 100 s obtained from turbidity measurements and suggests that Phe mode intensity increase and the turbidity data are monitoring the same process.

Comparison of Early Time Point Spectra and Small Aggregates. To understand the nature of the initial species observed in solution, we have compared spectra obtained at early times with those obtained from a sample containing small aggregates. The sample containing aggregates was prepared by cooling a polymerized sample to 4 °C for 2 h under deoxygenating conditions. The presence of small or seed aggregates was verified by reinitiating fiber formation through a temperature jump. Polymerization, followed by cooling of deoxy Hb S under the conditions defined for the time-resolved UVRR experiments, exhibited a decrease in the delay time by approximately 20% or greater (Table 1), demonstrating that the nucleation process is shortened consistent with earlier studies (*44*, *48*). In previous

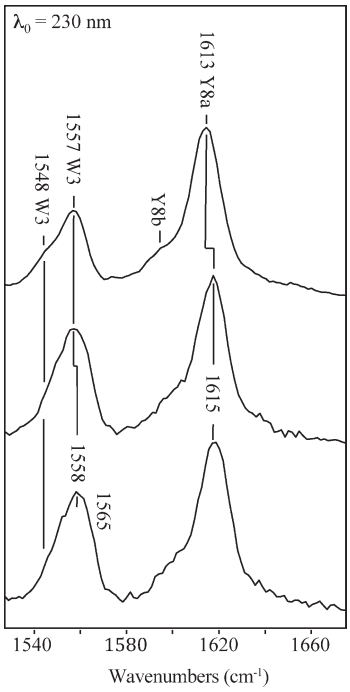

FIGURE 5: Expanded view of UVRR spectra obtained with 230 nm excitation showing the Y8a and W3 peaks. Spectra have been normalized to the intensity of the Y8a peak. Top: R-state spectrum. Center: Initial time point spectrum (deoxy Hb S tetramers). Bottom: Final time point spectrum (Hb S fibers).

reports shorter delay times were attributed to an increased concentration of aggregates or small polymers (*7*, *50*); therefore, in our case this reduction in the delay time is ascribed to the presence of aggregates, which have not completely dissociated during the cooling time period. The assignment is supported by the fact that if the samples are allowed to cool for longer periods of time such as overnight, repolymerization occurs on the prepolymerization time scale (data not shown). The aggregates are characterized as small because they do not lead to a detectable increase in sample turbidity (data not shown).

To examine the structure of these Hb S aggregates in solution, we obtained steady-state UVRR spectra of the solution before polymerization and following one cycle of polymerization and melting. The subsequent difference spectrum obtained at 4 °C, a temperature at which polymerization is not expected, shows an increase in Phe signal intensity (Figure 3d) similar to that obtained at early time points. If the polymers were completely melted, the spectra collected before and after polymerization would be expected to be exactly the same. The strong similarities in the small aggregate spectrum (Figure 3d) and early time point difference spectra (Figure 3a−c) are suggestive that the $\beta-\beta$ interaction is present in both cases and that the aggregates observed in the time-resolved experiments are similar to the prepared aggregates. The magnitude of the Phe intensity is larger for the prepared aggregates relative to those observed as a function of time. The greater Phe intensity results from either stronger interactions or a greater number of aggregates, which cannot be distinguished in the data obtained. Importantly, the UVRR spectra cannot detect the size of the aggregates, but the similarities of the difference spectra strongly suggest that the observed interactions are the same in both the preprepared and time-resolved cases and that even at the initial stages the molecular interactions are relatively ordered. These spectra point to an important role for the $\beta-\beta$ interaction in the early aggregates.

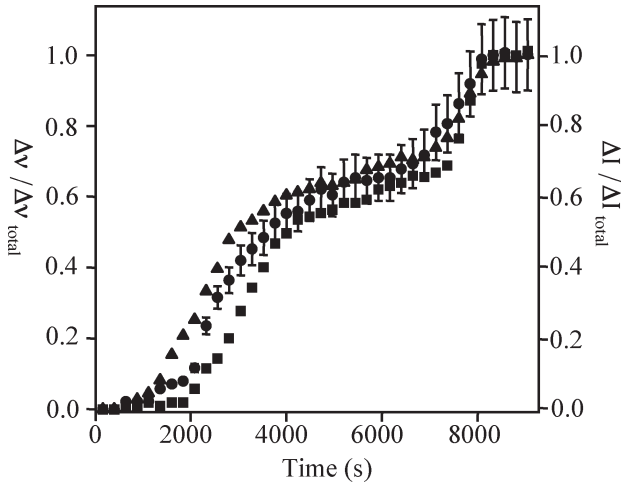

FIGURE 6: Kinetic progress curves constructed from the change in Y7a (circles) and Y8a (squares) frequency and W3 intensity (triangles) as a function of time. The left axis shows change in Y8a and Y7a frequency, and the right axis shows change in W3 intensity. Calculated $\Delta\nu$ was obtained relative to the Y8a and Y7a frequencies of the t_0 spectrum. Calculated W3 intensity was obtained by measuring the normalized intensity of the parent t_0 and t_f spectra. Two transitions were observed: one occurring at approximately 2040 s and one occurring at approximately 7340 s (see Table 1). For clarity, error bars are only shown for Y7a; however, the magnitude of the error is the same for all changes.

Dynamics of H-Bond Formation at the $\alpha_1\beta_2$ Interface. An excitation wavelength of 230 nm is used to monitor changes at the $\alpha_1\beta_2$ interface of hemoglobin. At this excitation wavelength Tyr and Trp residues are resonantly enhanced, and the observed bands have been previously assigned to the α42 Tyr and the β37 Trp residues, which form critical intersubunit H-bonds in the deoxy state (*33*, *51*, *52*). These changes are characterized by an increase in intensity of the Trp W3 mode and a frequency increase of the Tyr Y8a and Y8b modes (Figure 5), leading to a double derivative shape in the difference spectrum (Supporting Information Figure 1). Upon fiber formation a larger frequency shift of Tyr modes and greater intensity change of Trp modes are detected relative to deoxy tetramers and were attributed to a strengthening of T-state H-bonds at the $\alpha_1\beta_2$ interface in the fiber form (*37*, *38*). Comparison with difference spectra generated from equilibrium spectra of Hb S in the R, T, and F states demonstrates that the Hb S exists as unassociated deoxy monomers at the start of the measurements and as fibers at the end (Supporting Information Figure 2). An increase in intensity is also observed at 1565 cm^{-1}, which has been attributed to a strengthening of the β15 Trp−β72 Ser residue H-bond (Figure 5) (*31*, *33*, *36*, *38*). This interaction is strengthened in the fiber as the A-helix moves toward the interior of the tetramer as previously observed by X-ray crystallography (*2*).

Changes at the $\alpha_1\beta_2$ Interface Yield Two Transitions Associated with Fiber Formation. The changes in Tyr frequency (Y8a, Y7a) and Trp intensity (W3) as a function of time yield kinetic progress curves (Figure 6). In contrast to the Phe intensity curves, which show a single transition (Figure 4), the kinetic progress curves generated by monitoring Tyr mode frequency (Y8a, Y7a) or W3 intensity exhibit two distinct transitions. The overall magnitude of the frequency shift is the same as that observed in the steady-state experiments (2.1 cm^{-1}) (*37*, *38*); however, the presence of two transitions is suggestive that the strengthening of H-bonds at the $\alpha_1\beta_2$ interface occurs in stages.

Analysis of the transitions is accomplished by treating the transitions independently, and t_{50} values are assigned based on a

Boltzmann fit of the data (Supporting Information Figure 3). The magnitude of the change associated with the first midpoint is approximately 60% of the total transition, and the midpoint occurs at 2040 ± 160 s, which is approximately 300 s longer than the midpoint determined from the change in Phe signal intensity (1680 s) and approximately 400 s longer than the midpoint determined by monitoring sample turbidity (1560 s) (Table 1). These differences are larger than one standard deviation of the measurement and indicate that the strengthening of the $\alpha_1\beta_2$ interface occurs subsequent to the initial association of tetramers through the $\beta-\beta$ interaction.

The second transition, corresponding to approximately 35−40% of the total transition, occurs approximately 5000 s after the first transition with an average value of 7340 s. This second transition is consistently observed in the Tyr and Trp difference spectra but not in the Phe difference spectra or the turbidity curves (data not shown).

DISCUSSION

Molecular Interactions in the Early Aggregates. The association of Hb S tetramers to form fibers has been monitored using UVRR spectroscopy. These studies examine both intermolecular and intramolecular interactions of the tetramers and yield new insight into the molecular nature of the early aggregates and the association process of the fibers. At the initial stages of Hb S fiber formation both heterogeneous and homogeneous nuclei may be present; however, because of their relatively low populations, observation is limited and likely not detectable in UVRR spectra (*7*, *50*). Formation of metastable clusters in the initial stages of fiber formation has been previously detected using NMR spectroscopy (*53*), dynamic light scattering (*14*, *49*), and differential interference contrast microscopy (DIC) (*11*, *21*, *54*). In Hb S solutions the formation of these dense liquid clusters facilitates nucleation, while, in contrast, dense liquid clusters of Hb A do not exhibit polymerization (*54*, *14*). UVRR results are consistent with the formation of these clusters, and significantly, even at the relatively early time points, the UVRR data suggest that the $\beta-\beta$ donor−acceptor interaction is present, indicative of an ordered association of molecules even in the clusters.

In addition, changes at the $\beta\beta$ or lateral contacts are relatively constant at early times. These findings suggest that the interactions in these metastable clusters are mainly comprised of intermolecular ${}_1\beta^1-{}_2\beta^2$ interactions that are hydrophobic in nature and are relatively weak and transient. Comparison with aggregates generated from melted polymers confirms that these initial transient intermolecular associations ultimately lead to polymerization and underline the importance of the ordered nature of the clusters. The size of the these aggregates or the critical nucleus cannot be determined from the UVRR data; however, analyses of delay times determined from turbidity data taken at different Hb S concentrations suggest that the size of the nucleus is approximately 30 tetramers, consistent with earlier observations (*5*, *6*, *48*, *55*). This size would be large enough to support formation of a fiber from seven double strands. Since nucleation size is strongly dependent on Hb S concentration, at physiological concentrations the nucleus is predicted to be smaller, but potentially still large enough to lead to association of seven double strands.

Hb S Polymerization Occurs in Multiple Stages. In this study, kinetic progress curves of polymerization are constructed from different spectroscopic signals. A comparison of the time scale of polymerization as monitored by visible absorption spectroscopy, the intermolecular ${}^1\beta_1-{}^2\beta_2$ interaction, and the intramolecular $\alpha_1\beta_2$ interaction is strongly suggestive that Hb S fiber formation is a stepwise process (Table 1). The stepwise nature of the assembly was previously shown by DIC and electron microscopy experiments, which monitored the growth of fibers. These studies have shown that the fibers not only assemble to form twisted structures but also spontaneously assemble into branched fibers and fiber bundles, which occurs several minutes after initial fiber formation (*6*, *21*, *22*, *56*, *57*). UVRR results are generally consistent with the observation of higher order fiber structures following the formation of the initial fiber, although the timing of the electron microscopy and DIC experiments cannot be directly compared to the current work because of differences in reaction conditions.

From the X-ray crystallographic data and the electron micrographs of fibers, the molecular interactions observed in the crystal (*1*, *2*) can be extrapolated to intra- and inter-double-strand contacts observed in the fibers. UVRR measurements interpreted in terms of these interactions provide molecular insight into the assembly process. The increase in UVRR Phe intensities attributed to the ${}^1\beta_1-{}^2\beta_2$ interactions can be correlated with the lateral intra-double-strand contacts identified in electron micrographs and the X-ray data as shown in Figure 7a (*17*, *18*, *58*). These contacts, which flank the donor−acceptor interaction, appear to form early on in the association process. The observation of the increase in Phe intensities is nearly concomitant with the increase in sample turbidity (Table 1), which strongly supports a model where the lateral contacts are critical for Hb S tetramer−tetramer association. Over time these lateral contacts grow in number and strength as shown by the amplification of Phe signal intensity, consistent with the formation of increasingly larger polymers.

Evidence for a multistep polymerization process is found in the kinetic progress curves derived from signals associated with the $\alpha_1\beta_2$ and the symmetry-related $\alpha_2\beta_1$ interfaces, which yield an average delay time of 2040 s, substantively longer than that obtained from turbidity or Phe signal intensity. Thus, the strengthening of the H-bonds at this interface previously observed in equilibrium fiber spectra (*37*, *38*) occurs after formation of the initial ${}^1\beta_1-{}^2\beta_2$ contacts.

Although the $\alpha_1\beta_2$ and the $\alpha_2\beta_1$ interfaces are symmetry-related, the double strand contacts are not, and they potentially have a differential impact on the two interfaces (*58*). Both $\alpha_1\beta_2$ and $\alpha_2\beta_1$ interfaces are impacted by the lateral contacts that occur *between* the double strands of the fiber (shown in red) (Figure 7b,c) (*17*, *58*). Importantly, these contacts affect both the α42 Tyr−β99 Asp and β37 Trp−α94 Asp H-bonds, in contrast to the intrastrand contacts (green), which only impact the α42 Tyr H-bonds. These interfaces are not proximal to the axial contacts (blue) and are unlikely to be affected by those interactions. As shown in Figure 7b, lateral intra-double-strand interactions possibly influence the $\alpha_2\beta_1$ interaction only, and we suggest that the strengthening of the lateral contacts within a double strand (*17*, *18*, *58*) also leads to the strengthening of these critical H-bonds. This is not entirely unexpected as the hydrophobic EF corner, an important element of the lateral ${}^1\beta_1-{}^2\beta_2$ interaction, is in close spatial proximity to the β99 Asp residue, which forms a H-bond with the α42 Tyr residue. Similarly, residues 47−50 of the α_2 subunit are also identified in the lateral intra-double-strand contacts, which in turn can impact the α42 residue.

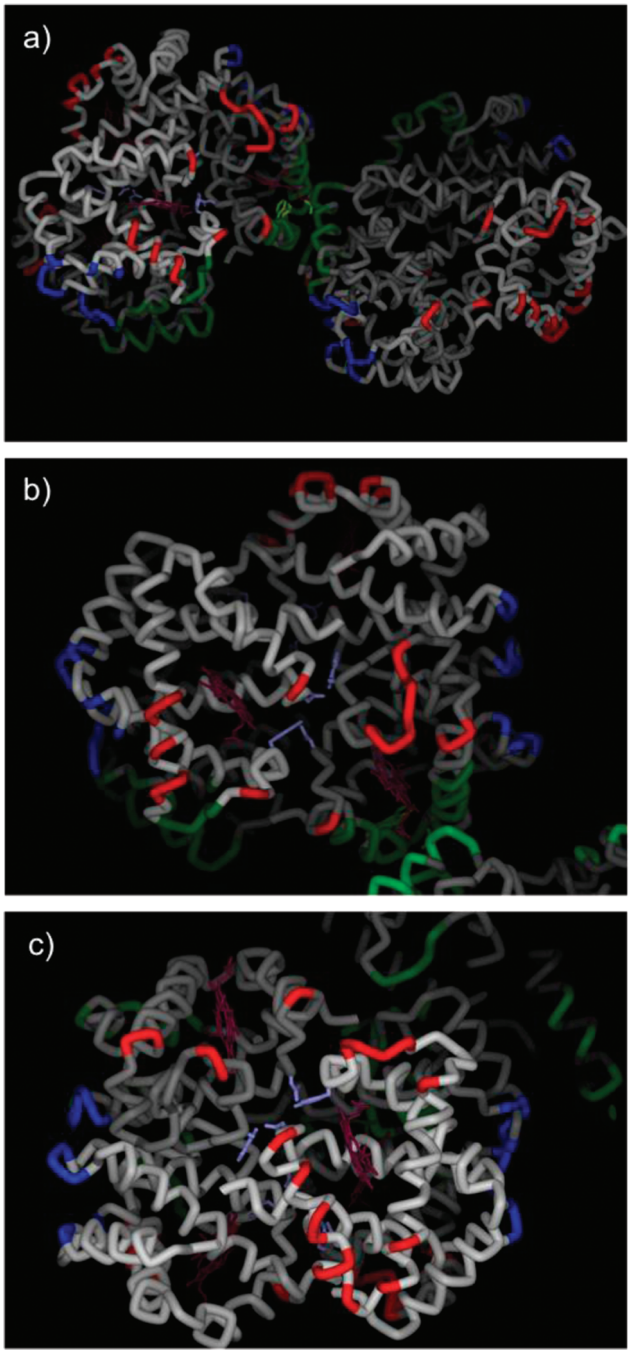

FIGURE 7: Contacts formed in the fibers are highlighted on the Hb S X-ray crystal structure. Intra-double-strand lateral contacts are shown in green, intra-double-strand axial contacts are shown in blue, and inter-double-strand lateral contacts are shown in red. The α subunits are shown in light gray, and the β subunits are shown in dark gray. (a) The lateral contact formed between the $^{2}\beta_{2}$6 Val, $^{1}\beta_{1}$85 Phe, and $^{1}\beta_{1}$88 Leu residues, which are shown in light green. (b) The $\alpha_2\beta_1$ interface with $\alpha_2$42 Tyr, $\beta_1$99 Asp, $\beta_1$37 Trp, and $\alpha_2$94 Asp residues shown in violet. (c) The $\alpha_1\beta_2$ interface with $\alpha_1$42 Tyr, $\beta_2$99 Asp, $\beta_2$37 Trp, and $\alpha_1$94 Asp residues shown in violet. For clarity, heme groups are shown on only one tetramer in maroon, and in (b) and (c) views are of the same tetramer. Figure prepared using Weblab Viewer.

With respect to the $\alpha_1\beta_2$ and $\alpha_2\beta_1$ interfaces, many points of contact from the inter-double-strand lateral interactions (red, Figure 7b,c) are observed on the surrounding helices, which potentially influence all four residues involved in these critical H-bonds. Time-resolved UVRR spectra monitoring the αβ intersubunit interface reveal that approximately 8000 s are required to obtain the structure previously observed by equilibrium UVRR experiments (*37*, *38*). A feature of the data reporting on this interface is an apparent second transition occurring at much longer times (> 7000 s). It is likely that the growth of fibers into larger structures constrains these inter-double-strand contacts, further solidifying these interfaces. Thus, we speculate that the first transition observed reports on the formation of initial fibers and fiber bundles and the second transition results from the formation of larger fiber aggregates, such as gels and macrofibers, which impact the lateral contacts between strands, strengthening the H-bonds across the $\alpha_1\beta_2$ and $\alpha_2\beta_1$ interfaces.

Mutational studies in conjunction with UVRR measurements have indicated that the β37 Trp H-bond is responsible for much of the quaternary constraint and reduced ligand affinity of the deoxy state (*51*). The reduced ligand affinity previously observed for Hb S fibers (*59*, *60*) is attributed to the increased stabilization of the $\alpha_1\beta_2$ interface within the fibers relative to individual deoxy tetramers. Importantly, the current study demonstrates that the last stages of the polymerization process continue to effectively reduce the O_2 affinity of Hb S fibers, suggesting a second time window for disrupting the fiber-forming process subsequent to the delay time.

Summary. A model for Hb S fiber assembly emerges from a consideration of the UVRR data in the context of the lateral interactions within the double strands and between the double strands, previously identified by electron microscopy and X-ray crystallography (Figure 7). These observations confirm the importance of the $^{1}\beta_{1}-^{2}\beta_{2}$ lateral contact for forming and stabilizing the initial aggregates and strands. Subsequent growth of the double strands and association into bundles and branched structures lead to a further strengthening of these lateral contacts through the twisting of the fibers, detected as an increase in Phe intensities and the strengthening of the $\alpha_2\beta_1$ and $\alpha_1\beta_2$ interfaces. Association of strands and fibers into macrofibers and larger structures occurs significantly later in the process and also leads to strengthening of H-bonds across these interfaces. The ability to monitor multiple regions of the molecule during fiber formation using UVRR spectroscopy yields considerable insight into the polymerization process and may represent another method to assess the mechanism and effectiveness of sickle cell disease treatments. We anticipate that these new insights into the mechanism of sickle cell fiber formation will inform the search for new therapies to combat sickle cell disease.

ACKNOWLEDGMENT

We are grateful to Drs. C. Alvin Head and Pedro Montero-Huerta (Medical College of Georgia) for providing us with blood from SS and SC patients. We thank Prof. Irina Russu for helpful discussions and critical reading of the manuscript.

SUPPORTING INFORMATION AVAILABLE

Figure 1, sickle cell Hb UVRR spectra, excited at 230 nm, at t_0, t_f and the associated difference spectrum; Figure 2, UVRR steady-state and time-resolved difference spectra obtained with 230 nm excitation comparing deoxy (T) and fiber (F) states with the fully liganded R state; Figure 3, kinetic progress curves of the Y8a, Y9a, and W3 vibrational modes with associated Boltzmann fits to the data. This material is available free of charge via the Internet at http://pubs.acs.org.

REFERENCES

1. Padlan, E. A., and Love, W. E. (1985) Refined crystal structure of deoxyhemoglobin S. II. Molecular interactions in the crystal. *J. Biol. Chem. 260*, 8280–8291.
2. Harrington, D. J., Adachi, K., and Royer, W. E., Jr. (1997) The high resolution crystal structure of deoxyhemoglobin S. *J. Mol. Biol. 272*, 398–407.
3. Harrington, D. J., Adachi, K., and Royer, W. E., Jr. (1998) Crystal structure of deoxy-human hemoglobin beta6 Glu → Trp. Implications for the structure and formation of the sickle cell fiber. *J. Biol. Chem. 273*, 32690–32696.
4. Mozzarelli, A., Hofrichter, J., and Eaton, W. A. (1987) Delay time of hemoglobin S polymerization prevents most cells from sickling in vivo. *Science 237*, 500–506.
5. Ferrone, F. A., Hofrichter, J., and Eaton, W. A. (1985) Kinetics of sickle hemoglobin polymerization. II. A double nucleation mechanism. *J. Mol. Biol. 183*, 611–631.
6. Eaton, W. A., and Hofrichter, J. (1990) Sickle cell hemoglobin polymerization. *Adv. Protein Chem. 40*, 63–279.
7. Ferrone, F. A. (2006) Nucleation: the connections between equilibrium and kinetic behavior. *Methods Enzymol. 412*, 285–299.
8. Ferrone, F. (1999) Analysis of protein aggregation kinetics. *Methods Enzymol. 309*, 256–274.
9. Galkin, O., Chen, K., Nagel, R. L., Hirsch, R. E., and Vekilov, P. G. (2002) Liquid-liquid separation in solutions of normal and sickle cell hemoglobin. *Proc. Natl. Acad. Sci. U.S.A. 99*, 8479–8483.
10. Galkin, O., Nagel, R. L., and Vekilov, P. G. (2007) The kinetics of nucleation and growth of sickle cell hemoglobin fibers. *J. Mol. Biol. 365*, 425–439.
11. Galkin, O., Pan, W., Filobelo, L., Hirsch, R. E., Nagel, R. L., and Vekilov, P. G. (2007) Two-step mechanism of homogeneous nucleation of sickle cell hemoglobin polymers. *Biophys. J. 93*, 902–913.
12. Galkin, O., and Vekilov, P. G. (2004) Mechanisms of homogeneous nucleation of polymers of sickle cell anemia hemoglobin in deoxy state. *J. Mol. Biol. 336*, 43–59.
13. Pan, W., Galkin, O., Filobelo, L., Nagel, R. L., and Vekilov, P. G. (2007) Metastable mesoscopic clusters in solutions of sickle-cell hemoglobin. *Biophys. J. 92*, 267–277.
14. Vaiana, S. M., Rotter, M. A., Emanuele, A., Ferrone, F. A., and Palma-Vittorelli, M. B. (2005) Effect of T-R conformational change on sickle-cell hemoglobin interactions and aggregation. *Proteins 58*, 426–438.
15. Sokolov, L., and Mukerji, I. (1998) Conformational changes in FmetHbS probed with UV resonance Raman and fluorescence spectroscopic methods. *J. Phys. Chem. B 102*, 8314–8319.
16. Carragher, B., Bluemke, D. A., Gabriel, B., Potel, M. J., and Josephs, R. (1988) Structural analysis of polymers of sickle cell hemoglobin. I. Sickle hemoglobin fibers. *J. Mol. Biol. 199*, 315–331.
17. Watowich, S. J., Gross, L. J., and Josephs, R. (1993) Analysis of the intermolecular contacts within sickle hemoglobin fibers: effect of site-specific substitutions, fiber pitch, and double-strand disorder. *J. Struct. Biol. 111*, 161–179.
18. Mu, X. Q., Makowski, L., and Magdoff-Fairchild, B. (1998) Analysis of the stability of hemoglobin S double strands. *Biophys. J. 74*, 655–668.
19. Turner, M. S., Briehl, R. W., Ferrone, F. A., and Josephs, R. (2003) Twisted protein aggregates and disease: the stability of sickle hemoglobin fibers. *Phys. Rev. Lett. 90*, 128101–128107.
20. Wang, Z., Kishchenko, G., Chen, Y., and Josephs, R. (2000) Polymerization of deoxy-sickle cell hemoglobin in high-phosphate buffer. *J. Struct. Biol. 131*, 197–209.
21. Briehl, R. W. (1995) Nucleation, fiber growth and melting, and domain formation and structure in sickle cell hemoglobin fibers. *J. Mol. Biol. 245*, 710–723.
22. Briehl, R. W., and Guzman, A. E. (1994) Fragility and structure of hemoglobin S fibers and their consequences for geleation kinetics and rheology. *Blood 83*, 573–579.
23. Balakrishnan, G., Weeks, C. L., Ibrahim, M., Soldatova, A. V., and Spiro, T. G. (2008) Protein dynamics from time resolved UV Raman spectroscopy. *Curr. Opin. Struct. Biol. 18*, 623–629.
24. Balakrishnan, G., Hu, Y., Bender, G. M., Getahun, Z., DeGrado, W. F., and Spiro, T. G. (2007) Enthalpic and entropic stages in alpha-helical peptide unfolding, from laser T-jump/UV Raman spectroscopy. *J. Am. Chem. Soc. 129*, 12801–12808.
25. Kneipp, J., Balakrishnan, G., Chen, R., Shen, T. J., Sahu, S. C., Ho, N. T., Giovannelli, J. L., Simplaceanu, V., Ho, C., and Spiro, T. G. (2006) Dynamics of allostery in hemoglobin: roles of the penultimate tyrosine H bonds. *J. Mol. Biol. 356*, 335–353.
26. Lednev, I. K., Karnoup, A. S., Sparrow, M. C., and Asher, S. A. (2001) Transient UV Raman spectroscopy finds no crossing barrier between the peptide alpha-helix and fully random coil conformation. *J. Am. Chem. Soc. 123*, 2388–2392.
27. Chi, Z., Chen, X. G., Holtz, J. S., and Asher, S. A. (1998) UV resonance Raman-selective amide vibrational enhancement: quantitative methodology for determining protein secondary structure. *Biochemistry 37*, 2854–2864.
28. Ahmed, Z., and Asher, S. A. (2006) UV resonance Raman investigation of a 3(10)-helical peptide reveals a rough energy landscape. *Biochemistry 45*, 9068–9073.
29. Friedman, J. M. (1994) Time-resolved resonance Raman spectroscopy as probe of structure, dynamics, and reactivity in hemoglobin. *Methods Enzymol. 232*, 205–231.
30. Samuni, U., and Friedman, J. M. (2005) Proteins in motion: resonance Raman spectroscopy as a probe of functional intermediates. *Methods Mol. Biol. 305*, 287–300.
31. Balakrishnan, G., Tsai, C. H., Wu, Q., Case, M. A., Pevsner, A., McLendon, G. L., Ho, C., and Spiro, T. G. (2004) Hemoglobin site-mutants reveal dynamical role of interhelical H-bonds in the allosteric pathway: time-resolved UV resonance Raman evidence for intra-dimer coupling. *J. Mol. Biol. 340*, 857–868.
32. Zhao, X., Balakrishnan, G., Moore, E. G., and Spiro, T. G. (2000) Kinetics of hemoglobin allostery from time-resolved UV resonance Raman spectroscopy: effect of a chemical cross link. *J. Raman Spectrosc. 31*, 349–352.
33. Rodgers, K. R., Su, C., Subramaniam, S., and Spiro, T. (1992) Hemoglobin R to T structural dynamics from simultaneous monitoring of tyrosine and tryptophan time-resolved UV resonance Raman signals. *J. Am. Chem. Soc. 114*, 3697–3709.
34. Kneipp, J., Balakrishnan, G., and Spiro, T. G. (2004) Time-resolved resonance Raman study of Hb A with 220 nm excitation: probing phenylalanine. *J. Phys. Chem. B 108*, 15919–15927.
35. Kitagawa, T., Haruta, N., and Mizutani, Y. (2002) Time-resolved resonance Raman study on ultrafast structural relaxation and vibrational cooling of photodissociated carbonmonoxy myoglobin. *Biopolymers 67*, 207–213.
36. Jayaraman, V., Rodgers, K. R., Mukerji, I., and Spiro, T. G. (1995) Hemoglobin allostery: resonance Raman spectroscopy of kinetic intermediates. *Science 269*, 1843–1848.
37. Knee, K. M., Roden, C. K., Flory, M. R., and Mukerji, I. (2007) The role of beta 93 Cys in the inhibition of Hb S fiber formation. *Biophys. Chem. 127*, 181–193.
38. Sokolov, L., and Mukerji, I. (2000) Structure of sickle cell hemoglobin fibers probed with UV resonance Raman spectroscopy. *J. Phys. Chem. B 104*, 10835–10843.
39. Xu, M., Shashilov, V. A., Ermolenkov, V. V., Fredriksen, L., Zagorevski, D., and Lednev, I. K. (2007) The first step of hen egg white lysozyme fibrillation, irreversible partial unfolding, is a two-state transition. *Protein Sci. 16*, 815–832.
40. Shashilov, V., Xu, M., Ermolenkov, V. V., Fredriksen, L., and Lednev, I. K. (2007) Probing a fibrillation nucleus directly by deep ultraviolet Raman spectroscopy. *J. Am. Chem. Soc. 129*, 6972–6973.
41. Balakrishnan, G., Case, M. A., Pevsner, A., Zhao, X., Tengroth, C., McLendon, G. L., and Spiro, T. G. (2004) Time-resolved absorption and UV resonance Raman spectra reveal stepwise formation of T quaternary contacts in the allosteric pathway of hemoglobin. *J. Mol. Biol. 340*, 843–856.
42. Antonini, E., and Brunori, M. (1971) Hemoglobin and Myoglobin in their Reactions with Ligands, Vol. 21, North-Holland, Amsterdam and London.
43. Ferrone, F. A., Hofrichter, J., and Eaton, W. A. (1985) Kinetics of sickle hemoglobin polymerization. I. Studies using temperature-jump and laser photolysis techniques. *J. Mol. Biol. 183*, 591–610.
44. Adachi, K., and Asakura, T. (1979) Nucleation-controlled aggregation of deoxyhemoglobin S. Possible difference in the size of nuclei in different phosphate concentrations. *J. Biol. Chem. 254*, 7765–7771.
45. Adachi, K., and Asakura, T. (1982) Kinetics of the polymerization of hemoglobin in high and low phosphate buffers. *Blood Cells 8*, 213–224.
46. Perutz, M. F., Fermi, G., Luisi, B., Shannan, B., and Liddington, R. C. (1987) Stereochemistry of cooperative mechanisms in hemoglobin. *Acc. Chem. Res. 20*, 309–321.
47. Adachi, K., Ding, M., Surrey, S., Rotter, M., Aprelev, A., Zakharov, M., Weng, W., and Ferrone, F. A. (2006) The Hb A variant (beta73 Asp→Leu) disrupts Hb S polymerization by a novel mechanism. *J. Mol. Biol. 362*, 528–538.

48. Yohe, M. E., Sheffield, K. M., and Mukerji, I. (2000) Solubility of fluoromethemoglobin S: effect of phosphate and temperature on polymerization. *Biophys. J. 78*, 3218–3226.
49. Chen, K., Ballas, S. K., Hantgan, R. R., and Kim-Shapiro, D. B. (2004) Aggregation of normal and sickle hemoglobin in high concentration phosphate buffer. *Biophys. J. 87*, 4113–4121.
50. Ferrone, F. A. (2004) Polymerization and sickle cell disease: a molecular view. *Microcirculation 11*, 115–128.
51. Kavanaugh, J. S., Rogers, P. H., Arnone, A., Hui, H. L., Wierzba, A., DeYoung, A., Kwiatkowski, L. D., Noble, R. W., Juszczak, L. J., Peterson, E. S., and Friedman, J. M. (2005) Intersubunit interactions associated with Tyr42 alpha stabilize the quaternary-T tetramer but are not major quaternary constraints in deoxyhemoglobin. *Biochemistry 44*, 3806–3820.
52. Nagai, M., Wajcman, H., Lahary, A., Nakatsukasa, T., Nagatomo, S., and Kitagawa, T. (1999) Quaternary structure sensitive tyrosine residues in human hemoglobin: UV resonance Raman studies of mutants at α140, β35 and β145 tyrosine. *Biochemistry 38*, 1243–1251.
53. Russu, I. M., and Ho, C. (1980) Proton longitudinal relaxation investigation of histidyl residues of normal human adult and sickle deoxyhemoglobin: evidence for the existence of pregelation aggregates in sickle deoxyhemoglobin solutions. *Proc. Natl. Acad. Sci. U.S.A. 77*, 6577–6581.
54. Chen, Q., Vekilov, P. G., Nagel, R. L., and Hirsch, R. E. (2004) Liquid-liquid phase separation in hemoglobins: distinct aggregation mechanisms of the β6 mutants. *Biophys. J. 86*, 1702–1712.
55. Adachi, K., and Asakura, T. (1979) Gelation of deoxyhemoglobin A in concentrated phosphate buffer. *J. Biol. Chem. 254*, 12273–12276.
56. McDade, W. A., and Josephs, R. (1993) On the formation and crystallization of sickle hemoglobin macrofibers. *J. Struct. Biol. 110*, 90–97.
57. Carragher, B., Bluemke, D. A., Becker, M., McDade, W. A., Potel, M. J., and Josephs, R. (1988) Structural analysis of polymers of sickle cell hemoglobin. III. Fibers within fascicles. *J. Mol. Biol. 199*, 383–388.
58. Watowich, S. J., Gross, L. J., and Josephs, R. (1989) Intermolecular contacts within sickle hemoglobin fibers. *J. Mol. Biol. 209*, 821–828.
59. Sunshine, H. R., Hofrichter, J., Ferrone, F. A., and Eaton, W. A. (1982) Oxygen binding by sickle cell hemoglobin polymers. *J. Mol. Biol. 158*, 251–273.
60. Shapiro, D. B., Esquerra, R. M., Goldbeck, R. A., Ballas, S. K., Mohandas, N., and Kliger, D. S. (1995) Carbon monoxide religation kinetics to hemoglobin S polymers following ligand photolysis. *J. Biol. Chem. 270*, 26078–26085.